Langmuir

Article

pubs.acs.org/Langmuir

Interface Properties of Organic *para*-Hexaphenyl/α-Sexithiophene Heterostructures Deposited on Highly Oriented Pyrolytic Graphite

Günther Schwabegger,[†] Martin Oehzelt,[‡,§] Ingo Salzmann,[§] Francesco Quochi,[∥] Michele Saba,[∥] Andrea Mura,[∥] Giovanni Bongiovanni,[∥,⊥] Antje Vollmer,[‡] Norbert Koch,[‡,§] Helmut Sitter,[†] and Clemens Simbrunner*[,†,∥]

[†]Institute of Semiconductor and Solid State Physics, Johannes Kepler University, Altenbergerstrasse 69, A-4040 Linz, Austria

[‡]Helmholtz Zentrum Berlin für Materialien und Energie GmbH, BESSY II, D-12489 Berlin, Germany

[§]Institut für Physik, Humboldt-Universität zu Berlin, D-12489 Berlin, Germany

[∥]Dipartimento di Fisica, Università di Cagliari, I-09042 Monserrato (CA), Italy

[⊥]Istituto Officina dei Materiali (CNR-IOM), Unità di Cagliari, I-09042 Monserrato (CA), Italy

Supporting Information

ABSTRACT: It was recently reported, that heterostructures of *para*-hexaphenyl (p-6P) and α-sexithiophene (6T) deposited on muscovite mica exhibit the intriguing possibility to prepare lasing nanofibers of tunable emission wavelength. For p-6P/6T heterostructures, two different types of 6T emission have been observed, namely, the well-known red emission of bulk 6T crystals and additionally a green emission connected to the interface between p-6P and 6T. In this study, the origin of the green fluorescence is investigated by photoelectron spectroscopy (PES). As a prerequisite, it is necessary to prepare structurally similar organic crystals on a conductive surface, which leads to the choice of highly oriented pyrolytic graphite (HOPG) as a substrate. The similarity between p-6P/6T heterostructures on muscovite mica and on HOPG is evidenced by X-ray diffraction (XRD), scanning force microscopy (SFM), and optical spectroscopy. PES measurements show that the interface between p-6P and 6T crystals is sharp on a molecular level without any sign of interface dipole formation or chemical interaction between the molecules. We therefore conclude that the different emission colors of the two 6T phases are caused by different types of molecular aggregation.

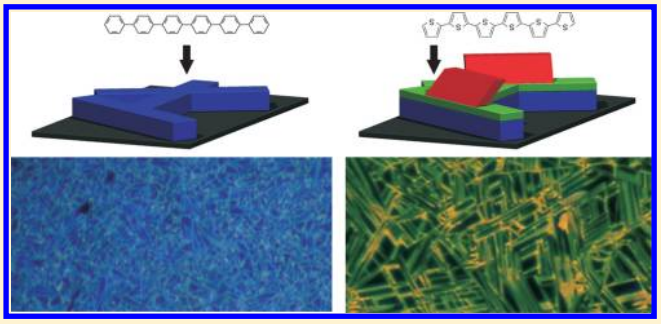

INTRODUCTION

During the last few years, the self-assembly of ordered structures on the nanoscale has been recognized as a key issue in nanotechnology, opening novel perspectives for device applications.[1−4] However, the development of structures that are confined in one or two dimensions remains a challenge that stimulates the scientific community to study and model the growth of various nanostructures, including nanowires,[5,6] quantum dots,[7,8] and nanocrystals.[9,10]

In addition to applications of inorganic nanostructures in nanomedicine[11,12] and nanoelectronics,[13,14] it was found that organic self-assembled nanostructures offer novel perspectives for device applications including optical sensors, waveguides, and laser sources.[15−18] A recent example is parallel para-hexaphenyl (p-6P) nanofibers that are prepared by vacuum deposition on muscovite mica substrates (sketched in Figure 1a), showing strong polarized blue fluorescence, waveguiding, and random lasing if excited by UV radiation.[16,18,19] The formation of parallel nanofibers based on rodlike molecules is linked to the epitaxial alignment of their long molecular axis (LMA) with respect to the mirror axis of the muscovite mica substrate surface.[20] If the LMA is not perpendicular or parallel

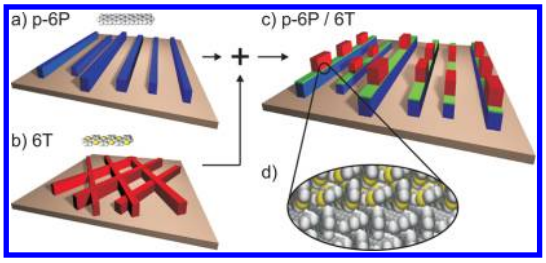

Figure 1. Sketch of self-assembled nanofibers prepared by vacuum deposition on muscovite mica. (a) Parallel fibers consisting of p-6P molecules. (b) Nonparallel fibers consisting of 6T molecules. (c) p-6P/6T heteroepitaxial fibers prepared by the deposition of 6T molecules on top of p-6P template fibers. 6T forms two different structures: an interface layer (green) and bulk crystallites (red). (d) Detailed view of the p-6P/6T interface showing the adaptation of the herringbone arrangement.[29,31]

Received: June 13, 2013
Revised: October 23, 2013
Published: October 25, 2013

   dx.doi.org/10.1021/la402242b | *Langmuir* 2013, 29, 14444−14450

to the surface mirror axis, then multiple fiber directions form as a result of a doubling of energetically equivalent adsorption geometries. Therefore, the preparation of parallel self-assembled nanofibers with significantly different optical properties (i.e., emitting in the visible green or red region) is not possible via simply replacing the molecular building blocks because the adsorption geometry is likewise altered. As sketched in Figure 1b for the case of sexithiophene (6T), such a strategy typically leads to multiple fiber directions and crossing points,[21−23] which reduces the length of the waveguides and, consequently, the accessible optical gain within the structures.

Heteroepitaxy of organic molecules can provide a solution to this problem because it influences the nucleation and ordering of organic adsorbate layers by the exploitation of templating effects.[24−27] For p-6P fibers, it was demonstrated that the emission spectrum can be tuned without disturbing the advantageous morphology and structure of the self-assembled nanofibers.[28−30] P-6P molecules are deposited on muscovite mica to prepare parallel crystalline structures, which act as templates for 6T molecules deposited subsequently (schematically depicted in Figure 1 c). The LMAs of 6T and p-6P molecules align parallel, and an adaptation of the specific herringbone packing of the two molecular species is observed.[29,31]

Remarkably, the photoluminescence spectrum of such heterostructures comprises not only blue p-6P and red 6T emission but also an additional contribution in the green spectral regime, which is related to the interface layer.[29] 6T molecules that are in direct contact with the p-6P crystals exhibit strikingly different optical properties as compared to bulk 6T crystals nucleating on top of p-6P fibers, with the green interfacial emission being significantly stronger than the red emission of bulk 6T. This finding motivated the use of multilayer structures of p-6P/6T to increase the green 6T contribution to the emission spectrum enabling random lasing in the green spectral regime.[32]

Here, we aim to identify and understand the origin of green 6T emission by investigating the electronic structure of the p-6P/6T interface using photoelectron spectroscopy (PES) because this technique is highly surface-sensitive and therefore ideal for studying submonolayer coverage as in the case of the evolvement of the p-6P/6T interface layer. In addition, chemical interactions between molecules can be studied with high precision, which allows us to answers the following questions: (1) Does intermixing of the two molecular species occur, leading to 6T molecules embedded in a p-6P matrix, which provides a significantly different environment compared to that of bulk, crystalline 6T? (2) Are additional interfacial electronic states present as a result of a strong interaction between p-6P and 6T molecules?

For PES measurements, electrically conductive substrates are indispensable to avoiding charging issues, which render the insulator muscovite mica an inappropriate substrate. However, to ensure the comparability of the results, an alternative substrate should allow p-6P and 6T crystallites to grow nanoneedles with the same contact planes as on muscovite mica (i.e., $(11\bar{1})_{6P}$, $(11\bar{2})_{6P}$, and $(\bar{4}11)_{6T}$).[31,33] Unfortunately, metal surfaces cannot be used because strong molecule−substrate interactions lead to the stabilization of different contact planes.[34−36] A substrate that is conductive and exhibits a lower substrate−molecule interaction but still stabilizes p-6P molecules in a flat-lying orientation[37−40] is highly oriented pyrolytic graphite (HOPG). Consequently, HOPG represents an ideal model system to replace muscovite mica in order to study the organic−organic interface properties by PES.

In this article, we first provide evidence by X-ray diffraction (XRD) that p-6P/6T crystals deposited on HOPG indeed exhibit similar crystal phases and contact planes as on muscovite mica. Subsequently, the morphological and optical properties of p-6P/6T bilayers on HOPG are investigated by scanning force microscopy (SFM) and fluorescence microscopy. Finally, the interface energy levels of p-6P/6T heterostructures are investigated by ultraviolet photoelectron spectroscopy (UPS) and X-ray photoelectron spectroscopy (XPS).

STRUCTURAL INVESTIGATIONS

XRD measurements were carried out to study the growth of p-6P and 6T on HOPG; a sketch of the samples is shown in Figure 2a.

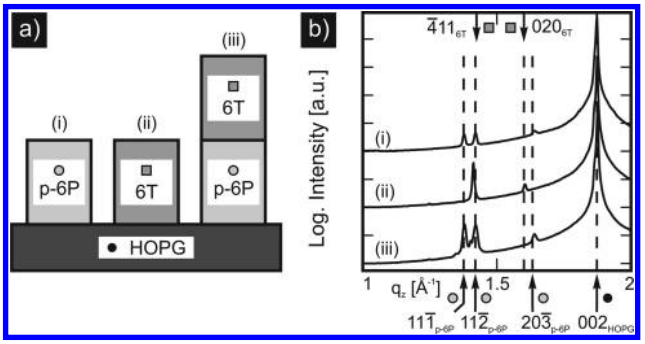

Figure 2. (a) Sketch of the sample structures including the symbols used for the indication of p-6P (gray circle), 6T (gray square), and HOPG (black circle) diffraction peaks. (b) Specular XRD of p-6P (i), 6T (ii), and p-6P/6T (iii) deposited on HOPG. Arrows and dashed lines indicate the peak positions for $(11\bar{1})_{p-6P}$, $(11\bar{2})_{p-6P}$, $(20\bar{3})_{p-6P}$, $(\bar{4}11)_{6T}$, $(020)_{6T}$, and $(002)_{HOPG}$, respectively; curves are shifted vertically for clarity.

p-6P (60 nm) was deposited on HOPG in the first step. The corresponding specular diffraction pattern is depicted in Figure 2b(i) as a function of the vertical component of the scattering vector (q_z) and shows four distinct peaks. The most intense reflection at q_z = 1.87 Å^{-1} is assigned to the (002) peak of the HOPG substrate. The peaks at q_z = 1.38, 1.42, and 1.63 Å^{-1} can be assigned to the $(11\bar{1})$, $(11\bar{2})$, and $(20\bar{3})$ diffraction peaks of the p-6P β-phase, respectively.[41,42] All three observed crystal orientations of p-6P originate from flat-lying molecules, and the more intense ones [$(11\bar{1})$ and $(11\bar{2})$] are likewise present on HWE-grown films on mica. Note that when taking the respective structure factors into account, $(20\bar{3})$ is clearly the minority species in the film.

In the next step, 6T (400 nm) was deposited on HOPG and analyzed by specular XRD. The spectrum in Figure 2b(ii) shows the presence of two reflections assigned to 6T in its so-called low-temperature (LT) phase.[43] The diffraction patterns can be well explained by crystals with $(\bar{4}11)$ and (010) contact planes observed at q_z = 1.42 and 1.60 Å^{-1}, respectively. Both crystal configurations are characteristic of flat-lying 6T molecules on the substrate surface, which agrees well with earlier reports from high-resolution electron energy loss spectroscopy.[44] No indications for upright-standing molecules

dx.doi.org/10.1021/la402242b | Langmuir 2013, 29, 14444−14450

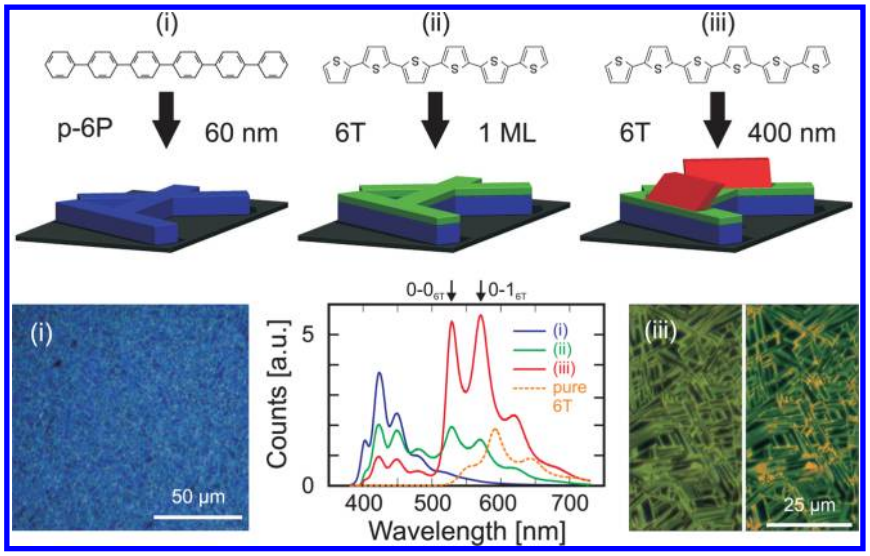

Figure 3. Sketch of the investigated sample structures. In the first step, nominally 60 nm p-6P was deposited on HOPG (i). Subsequently, nominally one monolayer of 6T was deposited on top of the p-6P template (ii). Finally, a 400-nm-thick 6T layer was grown on the p-6P template (iii), and all samples were characterized by fluorescence microscopy and photoluminescence (PL). A PL spectrum of pure 6T bulk crystallites is plotted as a reference. To resolve the relatively weakly emitting 6T crystallites, the red detection channel was amplified in the right panel of the color image acquired on sample iii.

are observed, which would be typically represented by a (100) contact plane.[22]

In a final step, 6T/p-6P/HOPG heterostructures were fabricated by preparing a nominally 60-nm-thick p-6P template. Subsequently, 6T was deposited without breaking the vacuum by choosing the same growth parameters as used for the preparation of the pure 6T film; the corresponding specular XRD data is shown in Figure 2b(iii). The presence of p-6P crystallites in the β phase is confirmed, and all p-6P crystal orientations (as discussed for pure 6P on HOPG) are observed. From 6T, only a small contribution of the $(\bar{4}11)_{6T}$ orientation is observed (seen as a shoulder at lower q_z next to the $(11\bar{2})_{p-6P}$ peak), whereas crystallites with a $(010)_{6T}$ orientation are absent. To verify the orientation of 6T, gracing-incidence reciprocal space maps (RSM) were recorded, which fully confirms our assignment (Supporting Information).

In summary, XRD provides a consistent picture that shows that p-6P crystallizes in the β phase whereas 6T molecules pack in their so-called LT phase. Both p-6P and 6T form multiple crystal orientations on HOPG, which all are indicative of flat-lying molecules with respect to the substrate surface. The molecular orientations of both the pure compounds and the heterostructures on HOPG are fully in line with what is observed for mica. As a consequence, HOPG seem to be perfectly suitable for studying the p-6P/6T interface with PES methods by analogy to muscovite mica.

MORPHOLOGY AND OPTICAL CHARACTERIZATION

Fluorescence microscopy represents an excellent method for combining morphological and optical investigations. By using an ultraviolet (UV) light source, the organic thin films are excited such that we can study their spatially resolved fluorescence. As indicated in Figure 3, a 60-nm-thick p-6P template layer was grown by HWE on HOPG as the first step (i) and analyzed by fluorescence microscopy showing strong blue emission. The photoluminescence (PL) spectra are consistent with literature data obtained for p-6P nanofibers on mica substrates.[18] The corresponding micrograph presented in Figure 3i reveals a netlike structure of p-6P nanofibers, which homogeneously cover the HOPG surface. This is consistent with our structural analysis because p-6P tends to form needlelike structures with $(11\bar{1})$ and $(11\bar{2})$ textures.[29,33] The low azimuthal anisotropy, in comparison to that of parallel-aligned p-6P nanofibers on mica, is attributed to the hexagonal substrate surface unit cell and to the fiber texture of HOPG. Consequently, p-6P nanofibers can be expected to show random azimuthal orientations on a macroscopic length scale, leading to the formation of a netlike sample morphology.

In step ii, nominally 0.4 nm 6T was deposited on the p-6P/HOPG template; the 6T layer thickness corresponds to approximately one monolayer (ML). As is clearly evident from the PL spectrum (green line in Figure 3), the fluorescence emission of the sample changes significantly. Beside the blue p-6P emission, a second band arises in the green spectral range. Note that comparable spectra were reported for such heterostructures grown on mica, where the presence of a 6T layer sensitized by the excited p-6P material via resonance-energy transfer was suggested.[29]

Having established the interfacial layer, 6T deposition was continued to nominally 400 nm of 6T (iii), and as indicated in Figure 3 (red line), the emission is altered again. In particular, the change in the intensity ratio of the 0−0 and 0−1 vibronic peaks (occurring at approximately 530 and 570 nm, respectively) was also observed in nanofibers fabricated on mica with comparable 6T thicknesses and was explained by a superposition of crystalline and interfacial 6T emissions.[29] From Figure 3iii, it is evident that the blue luminescence of p-6P is efficiently quenched and homogeneously green-emitting nanofibers are observed. In the right part of Figure 3iii, inhomogeneously distributed structures can be resolved on top of the nanofibers, which we attribute to the nucleation of 6T bulk crystallites emitting in the red-orange spectral range. It has to be stated that the red-orange emitting crystallites can be detected only if the red channel of the image is amplified. The weak PL emission of pure 6T crystallites exhibits its maximum

dx.doi.org/10.1021/la402242b | *Langmuir* 2013, 29, 14444−14450

intensity at higher wavelengths (dashed orange line in Figure 3), and this contribution is responsible for the increase of the 0−1 peak intesity of spectrum iii.

In addition, scanning force microscopy (SFM) images of the 6T/p-6P bilayer structure are shown in Figure 4a. At first glance, the netlike fiber morphology is reproduced from fluorescence microscopy. Flat regions are observed between the fibers, which can be attributed to the bare HOPG substrate (labeled A). In addition, two different needlelike morphologies are observed. Structures with height levels of approximately 60 nm nicely agree with the expected height of the p-6P template fibers (B), which exhibit a rectangular cross-section with a flat top, as seen in Figure 4b. On top of the p-6P crystallites, 140−400-nm-high entities are present (C), which exhibit a triangular cross section. As indicated by a dashed line in the height profile of Figure 4b, the flatter side facet of structures C exhibits an angle of ∼113° relative to the HOPG substrate surface. Recently, it was demonstrated by cross-sectional transmission electron microscopy (TEM) that 6T crystallites with a $(\bar{4}11)$ contact plane tend to form strongly tilted lamella-like structures.[29] This tilt was explained by an area maximization of the (100) low-energy plane, which forms the side walls of the 6T crystallites. As sketched in Figure 4c, the angle enclosing the side facet and the contact plane is given by 112.7°. Consequently, the experimental value agrees with that theoretically expected, which confirms that structures C reflect the morphology of $(\bar{4}11)$-oriented 6T crystallites. Note that previous TEM investigations revealed that such SFM cross sections reproduce only one facet correctly because of the finite cone angle of the tip.[29]

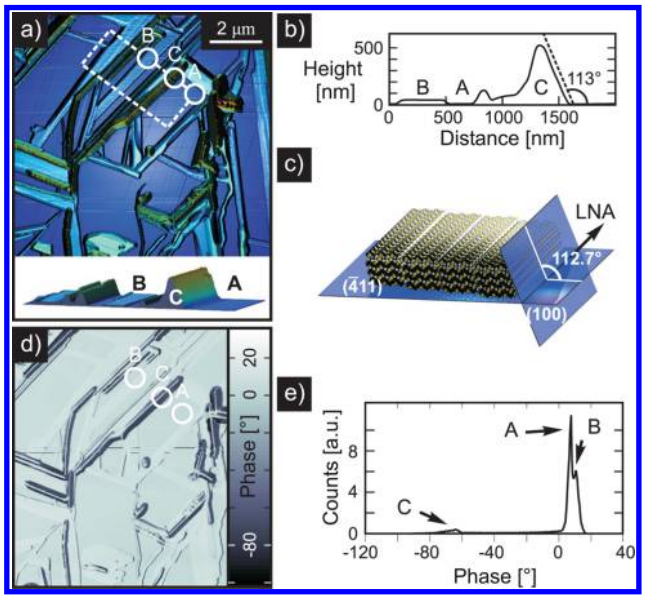

Figure 4. (a) Color-coded height image obtained by scanning force microscopy (SFM) on a nominally 400-/60-nm-thick 6T/p-6P heterostructure on HOPG. The cross section depicted below is taken from the region marked by a dashed polygon, and the corresponding height profile is presented in panel b. (c) Geometrical alignment of the (100) low-energy plane of $(\bar{4}11)$ 6T crystallites. The long needle axis (LNA) that is almost perpendicular to the long molecular axis (LMA) is indicated. (d) Color-coded phase image acquired at the same sample position indicating the presence of three different phase levels that are reflected by histogram peaks presented in panel e. Peak positions can be correlated with the HOPG substrate surface (A), rectangular p-6P template fibers (B), and triangularly shaped 6T fiber structures (C).

A simultaneously acquired phase image is presented in Figure 4d. Phase images provide information on local variations in the mechanical properties due to material-dependent dissipative processes related to the tip−sample interaction.[45−47] The measurement shows a positive phase shift for the HOPG (A) and p-6P template nanofibers (B). On the contrary, structures that were assigned to $(\bar{4}11)_{6T}$ crystallites cause a negative phase shift (visualized by dark regions). This observation is further substantiated by the phase histogram in Figure 4e, indicating three dominant phase levels that can be attributed to HOPG (A), p-6P template fibers (B), and 6T crystallites (C).

Photoelectron Spectroscopy. After evidencing the structural comparability between the p-6P/6T crystals on HOPG and mica, we now turn to the investigation of their electronic structure by UPS and XPS.

The measurements were carried out in the form of a thickness series, starting with a 5 -nm-thick p-6P layer and 6T layers deposited subsequently onto this template. The UPS valence band (VB), the secondary electron cutoff (SECO) spectra, and the XPS core-level spectra of carbon 1s (C 1s) and sulfur 2p (S 2p) were recorded for each thickness level (Figure 5). In the VB region, a peak around 3.3 eV binding energy (BE) is observed, which is assigned to the HOPG substrate. Upon p-6P deposition, two distinct peaks arise at 2.1 and 2.7 eV BE. These peaks are assigned to the p-6P HOMO and HOMO-1, respectively. (See the schematic energy-level diagram in Figure 5.) Upon 6T deposition, a new peak emerges at 1.4 eV that originates from the 6T HOMO and is clearly visible at a nominal thickness of only 0.2 nm 6T. Note that the BE of 6T HOMO-1 almost coincides with the HOMO of p-6P. With increasing 6T thickness, the peak at 1.4 eV increases in intensity, whereas the p-6P HOMO-1 peak becomes significantly attenuated. This points toward a sharp interface between p-6P and 6T because UPS is a highly surface-sensitive technique with an escape depth for electrons on the order of 1 nm at the given photon energy.[48] At a nominal 6T thickness of 1.6 nm, HOMO-1 of p-6P has almost vanished. Clearly, 6T grows on p-6P and completely covers the template layer.

The SECO shows that all interfaces are vacuum-level aligned because in the cutoff region essentially no shifts are observed.[49] Additionally, no shifts in BE are observed for either the VB region (UPS) or the core levels (XPS). In combination with the results from the VB region, a schematic energy-level diagram can be drawn (Figure 5, right). The HOMO onset positions (with respect to the Fermi level) and the ionization potentials (IP) are in good agreement with previous PES studies on individual layers of 6T[50] and p-6P.[51,52] The IPs and the HOMO onset for 6T (p-6P) are found to be at 5.4 eV (6.0 eV) and 0.9 eV (1.7 eV), respectively.

The observation of vacuum-level alignment and the absence of new electronic states, resulting from strong electronic coupling between the individual materials, clearly rules out that the observed green emission of a 6T ML on top of p-6P template crystals originates from interfacial electronic states.

■ SUMMARY AND CONCLUSIONS

The growth of p-6P, 6T, and 6T/p-6P heterostructures on HOPG was investigated. On the basis of X-ray diffraction measurements, it is shown that p-6P tends to crystallize in the β phase whereas 6T molecules pack in their so-called LT phase. p-6P crystallizes, when deposited on HOPG, in three different

dx.doi.org/10.1021/la402242b | Langmuir 2013, 29, 14444−14450

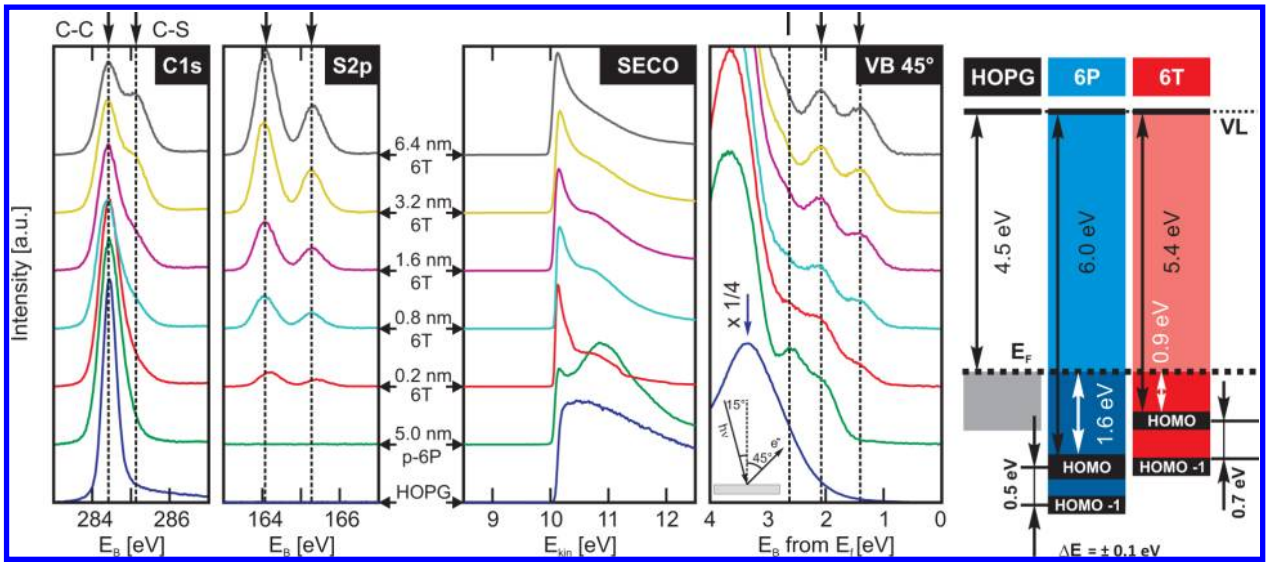

Figure 5. XPS and UPS spectra of the 6T/p-6P/HOPG heterostructure. p-6P (5 nm, green curve) is deposited on the bare HOPG substrate (blue). Layers of increasing 6T thickness are deposited onto the p-6P buffer layer with nominal thicknesses of 0.2 (red), 0.8 (cyan), 1.6 (magenta), 3.2 (yellow), and 6.4 nm (black). The left part of the figure shows the C 1s and S 2p core levels, the middle part shows the valence band region (takeoff angle of 45°) together with the secondary electron cutoff (SECO), and the right part shows a schematic energy-level diagram with energy values deduced from UPS.

geometries with $(11\bar{1})$, $(11\bar{2})$, and $(20\bar{3})$ contact planes parallel to the substrate surface. For 6T crystals, $(\bar{4}11)$ and (010) textured films are observed. Although $(\bar{4}11)$-oriented 6T crystallites also grow on the p-6P template, the (010) orientation vanishes. It seems that 6T crystallizes exclusively on top of the p-6P needles where 6T molecules adopt the herringbone arrangement of the underlying $(11\bar{1})_{6P}$ surface.[29,31] SFM investigations reveal three different sample morphologies, which are attributed to the HOPG substrate surface, the p-6P template fibers, and the 6T crystallites with a $(\bar{4}11)$ contact plane.

By combining PL and fluorescence microscopy, we demonstrate that 6T/p-6P heterostructures deposited on HOPG behave analogously to 6T/p-6P nanofibers on muscovite mica. Both homogeneous green-emitting interfacial 6T phase for low 6T coverages and red-emitting crystallites on top of p-6P structures are observed.

PES measurements show that the interface between p-6P and 6T is sharp on a molecular level, despite the reported tendency of mixed crystal formation upon vacuum codeposition.[53] Importantly, no indication of the presence of new electronic states is found in UPS. Vacuum-level alignment and therefore the absence of interface dipoles are observed. Consequently, the 6T molecules are physisorbed on top of p-6P crystals, and the green color of the 6T interface layer emission is not caused by ground-state electronic coupling with p-6P at the interface but rather resembles the spectrum of isolated 6T molecules both in solution[54] and in the submonolayer range of 6T on silicon dioxide.[55,56]

The interface layer preserves its optical emission characteristics even for large 6T thicknesses, where red-emitting bulk 6T crystals are formed. Sexithiophene deposited on *para*-hexaphenyl is thus understood to coexist in two different types of aggregation as similarly reported for 6T grown on silicon dioxide[55] or single-crystalline Cu.[57] In the interface layer, 6T molecules are characterized by weak intermolecular interactions, whereas in the overlying bulk crystals side-by-side interactions of 6T molecules dominate (H aggregation). H aggregates exhibit a low PL quantum yield with a forbidden 0−0 transition,[58] which is perfectly in line with our observations for bulk crystals of 6T on top of p-6P. In contrast, weakly interacting molecules feature an allowed 0−0 transition[56] and a high PL quantum yield. As a consequence, an inversion of the 0−0 to 0−1 emission intensity ratio can be observed as compared to large (400 nm) 6T coverages.

The growth analogy of p-6P/6T on HOPG and mica demonstrated in this study represents a straightforward approach to the investigation of the electrical properties of organic nanostructures grown on mica. In addition, it can open pathways for future optoelectronic devices based on intensively studied nanofibers of p-6P/6T . Such devices could be fabricated on transparent graphene electrodes instead of mica because the HOPG surface and graphene sheets allow the formation of structurally equivalent organic nanostructures as recently demonstrated.[59]

EXPERIMENTAL PROCEDURE

Hot Wall Epitaxy. All samples were fabricated on highly oriented pyrolytic graphite (HOPG) (001) of ZYA quality, and vacuum deposition of organic molecules was performed by hot wall epitaxy (HWE).[60] Immediately after being cleaved (using Scotch tape), the substrates were transferred via a load lock to the growth chamber, providing two separated HWE reactors equipped with p-6P (TCI) and 6T (Sigma-Aldrich) source material. The system was operated under high-vacuum (HV) conditions with a nominal pressure of 9×10^{-6} mbar. p-6P (6T) was evaporated at a temperature of 240 °C (190 °C), which resulted in a nominal growth rate of 1 nm/min (4.5 nm/min). To avoid temperature gradients during growth and to reduce adsorbed species on the surface, the substrate was preheated to 120 °C for 30 min and the temperature was kept constant during the whole growth procedure. After depositing p-6P for 60 min (~60 nm fiber height), the sample was automatically transferred under HV conditions to the 6T source oven. Subsequently, 6T was deposited for 1 s up to 90 min (~405 nm); the nominal layer thickness is defined as the average fiber height.

X-ray Diffraction. Specular X-ray diffraction measurements were performed at synchrotron radiation source HASYLAB (Hamburg, Germany) using a wavelength of 1.1771 Å. The W1 end-station is

dx.doi.org/10.1021/la402242b | *Langmuir* 2013, 29, 14444−14450

equipped with a pseudo-z-axis goniometer and a MYTHEN linear detector that spans ±2.3° in 2Θ. Every specular scan therefore yields a rocking curve at each value of the out-of-plane component of the scattering vector (q_z).

The reciprocal space maps (RSM) were measured in grazing incidence geometry with the linear detector oriented in the q_z direction. An RSM represents a 2D cut of the reciprocal space, where each reflection corresponds to a ring-shaped diffraction maximum in reciprocal space, which originates from the fiber texture of the HOPG substrate.[59]

The parameters of the monoclinic unit cell of p-6P (6T) used for peak assignment are a = 8.091 Å, b = 5.568 Å, c = 26.241 Å, and β = 98.17°[41,42] (a = 44.708 Å, b = 7.851 Å, c = 6.029 Å, and β = 90.76°[43]).

Morphological Investigations. Scanning force microscopy (SFM) studies were performed using a Digital Instruments Dimension 3100 in tapping mode. The SFM characterization was performed on an area of 10 × 10 μm^2 with a SiC tip.

Photoluminescence. Epifluorescence images were acquired upon sample illumination with a Hg lamp spectrally narrowed in the 330–360 nm band. For fluorescence spectroscopy, samples were excited over a large area of some hundreds of squared micrometers at 375 nm by a frequency-doubled Ti/sapphire oscillator with an 82 MHz repetition frequency. Emission was analyzed in a grating spectrometer and detected with a liquid-nitrogen-cooled detector.

Photoelectron Spectroscopy. PES experiments were carried out at end-station SurICat (at beamline PM4) at BESSY II (Berlin, Germany). The highly oriented pyrolytic graphite (HOPG) substrate for the UPS measurements was of ZYA quality and was preheated to 700 K for approximately 15 h. The p-6P and 6T molecules were evaporated from a Knudsen cell. The HOPG substrates were kept at room temperature during evaporation, and the deposition rates were ca. 1 Å/min. The film thicknesses given in the text are nominal mass–thickness values determined with a quartz crystal microbalance. Film deposition and UPS measurements were made in vacuum, and sample transfer did not break the vacuum. The PES spectra were collected with a hemispherical electron energy analyzer (Scienta SES 100) and an excitation energy of 18 eV at a 45° emission angle. The secondary electron cutoff (SECO) was measured at normal emission with an applied voltage of −10 V. The C 1s and S 2p core levels were investigated by XPS with a photon energy of 600 eV.

■ ASSOCIATED CONTENT

Ⓢ Supporting Information

XRD data (reciprocal space maps) of p-6P, 6T, and p-6P/6T bilayers grown on HOPG and full UPS spectra. This material is available free of charge via the Internet at http://pubs.acs.org.

■ AUTHOR INFORMATION

Corresponding Author

*E-mail: clemens.simbrunner@jku.at.

Notes

The authors declare no competing financial interest.

■ ACKNOWLEDGMENTS

This work has been financially supported by the Austrian Science Fund (FWF projects NFN-S9706 and P25154-N20) and by the federal government of Upper Austria (project Organische Nanostrukturen). C.S. acknowledges financial support as a visiting professor at the University of Cagliari (Programma Visiting Professor 2011/2012) supported by Regione Autonoma della Sardegna (contract no. 348/21727). We thank W. Caliebe (HASYLAB, Hamburg, Germany) for experimental support.

■ REFERENCES

(1) Whitesides, G. M.; Mathias, J. P.; Seto, C. T. Molecular self-assembly and nanochemistry - a chemical strategy for the synthesis of nanostructures. *Science* **1991**, *254*, 1312–1319.

(2) Barth, J. V.; Costantini, G.; Kern, K. Engineering atomic and molecular nanostructures at surfaces. *Nature* **2005**, *437*, 671.

(3) Li, R.; Hu, W.; Liu, Y.; Zhu, D. Micro- and nanocrystals of organic semiconductors. *Acc. Chem. Res.* **2010**, *43*, 529–540.

(4) Pileni, M. P. Supra- and nanocrystallinity: specific properties related to crystal growth mechanisms and nanocrystallinity. *Acc. Chem. Res.* **2012**, *45*, 1965–1972.

(5) Huang, M. H.; Mao, S.; Feick, H.; Yan, H.; Wu, Y.; Kind, H.; Weber, E.; Russo, R.; Yang, P. Room-temperature ultraviolet nanowire nanolasers. *Science* **2001**, *292*, 1897.

(6) Gudiksen, M. S.; Lauhon, L. J.; Wang, J.; Smith, D. C.; Lieber, C. M. Growth of nanowire superlattice structures for nanoscale photonics and electronics. *Nature* **2002**, *415*, 617.

(7) Stangl, J.; Holy, V.; Bauer, G. Structural properties of self-organized semiconductor nanostructures. *Rev. Mod. Phys.* **2004**, *76*, 725.

(8) Ustinov, V. M.; Maleev, N. A.; Zhukov, A. E.; Kovsh, A. R.; Egorov, A. Y.; Lunev, A. V.; Volovik, B. V.; Krestnikov, I. L.; Musikhin, Y. G.; Bert, N. A.; Kopev, P. S.; Alferov, Z. I.; Ledentsov, N. N.; Bimberg, D. InAs/InGaAs quantum dot structures on GaAs substrates emitting at 1.3 μm. *Appl. Phys. Lett.* **1999**, *74*, 2815.

(9) Pinna, N.; Weiss, K.; Sack-Kongehl, H.; Vogel, W.; Urban, J.; Pileni, M. P. Triangular CdS nanocrystals: synthesis, characterization, and stability. *Langmuir* **2001**, *17*, 7982–7987.

(10) Yarema, M.; Pichler, S.; Kriegner, D.; Stangl, J.; Yarema, O.; Kirchschlager, R.; Tollabimazraehno, S.; Humer, M.; Häringer, D.; Kohl, M.; Chen, G.; Heiss, W. From highly monodisperse indium and indium tin colloidal nanocrystals to self-assembled indium tin oxide nanoelectrodes. *ACS Nano* **2012**, *6*, 4113–4121.

(11) Farokhzad, O. C.; Langer, R. Impact of nanotechnology on drug delivery. *ACS Nano* **2009**, *3*, 16–20.

(12) Ghosh, D.; Lee, Y.; Thomas, S.; Kohli, A. G.; Yun, D. S.; Belcher, A. M.; Kelly, K. A. M13-templated magnetic nanoparticles for targeted in vivo imaging of prostate cancer. *Nat. Nano* **2012**, *7*, 677–682.

(13) Cen, C.; Thiel, S.; Mannhart, J.; Levy, J. Oxide nanoelectronics on demand. *Science* **2009**, *323*, 1026–1030.

(14) Ionescu, A. M. Nanoelectronics: ferroelectric devices show potential. *Nat. Nano* **2012**, *7*, 83–85.

(15) Zang, L.; Che, Y.; Moore, J. S. One-dimensional self-assembly of planar π-conjugated molecules: adaptable building blocks for organic nanodevices. *Acc. Chem. Res.* **2008**, *41*, 1596–1608.

(16) Yanagi, H.; Morikawa, T. Self-waveguided blue light emission in p-sexiphenyl crystals epitaxially grown by mask-shadowing vapor deposition. *Appl. Phys. Lett.* **1999**, *75*, 187–189.

(17) Takazawa, K.; Kitahama, Y.; Kimura, Y.; Kido, G. Optical waveguide self-assembled from organic dye molecules in solution. *Nano Lett.* **2005**, *5*, 1293–1296.

(18) Quochi, F. Random lasers based on organic epitaxial nanofibers. *J. Opt.* **2010**, *12*, 024003.

(19) Balzer, F.; Bordo, V. G.; Simonsen, A. C.; Rubahn, H.-G. Optical waveguiding in individual nanometer-scale organic fibers. *Phys. Rev. B* **2003**, *67*, 115408.

(20) Simbrunner, C.; Nabok, D.; Hernandez-Sosa, G.; Oehzelt, M.; Djuric, T.; Resel, R.; Romaner, L.; Puschnig, P.; Ambrosch-Draxl, C.; Salzmann, I.; Schwabegger, G.; Watzinger, I.; Sitter, H. Epitaxy of rodlike organic molecules on sheet silicates - a growth model based on experiments and simulations. *J. Am. Chem. Soc.* **2011**, *133*, 3056–3062.

(21) Schiek, M.; Balzer, F.; Al-Shamery, K.; Lützen, A.; Rubahn, H.-G. Nanoaggregates from thiophene/phenylene co-oligomers. *J. Phys. Chem. C* **2009**, *113*, 9601–9608.

(22) Simbrunner, C.; Hernandez-Sosa, G.; Oehzelt, M.; Djuric, T.; Salzmann, I.; Brinkmann, M.; Schwabegger, G.; Watzinger, I.; Sitter, H.; Resel, R. Epitaxial growth of sexithiophene on mica surfaces. *Phys. Rev. B* **2011**, *83*, 115443.

(23) Schwabegger, G.; Djuric, T.; Sitter, H.; Resel, R.; Simbrunner, C. Morphological and structural investigation of sexithiophene growth on KCl (100). *Cryst. Growth Des.* **2012**, *13*, 536−542.
(24) Hinderhofer, A.; Schreiber, F. Organic-organic heterostructures: concepts and applications. *ChemPhysChem* **2012**, *13*, 628−643.
(25) Moret, M.; Borghesi, A.; Campione, M.; Fumagalli, E.; Raimondo, L.; Sassella, A. Organic-organic heteroepitaxy: facts, concepts and perspectives. *Cryst. Res. Technol.* **2011**, *46*, 827−832.
(26) Mannsfeld, S. C. B.; Leo, K.; Fritz, T. Line-on-line coincidence: a new type of epitaxy found in organic-organic heterolayers. *Phys. Rev. Lett.* **2005**, *94*, 056104.
(27) Koller, G.; Berkebile, S.; Krenn, J. R.; Netzer, F. P.; Oehzelt, M.; Haber, T.; Resel, R.; Ramsey, M. G. Heteroepitaxy of organic-organic nanostructures. *Nano Lett.* **2006**, *6*, 1207−1212.
(28) Hernandez-Sosa, G.; Simbrunner, C.; Sitter, H. Growth and optical properties of alpha-sexithiopene doped para-sexiphenyl nanofibers. *Appl. Phys. Lett.* **2009**, *95*, 013306.
(29) Simbrunner, C.; Quochi, F.; Hernandez-Sosa, G.; Oehzelt, M.; Resel, R.; Hesser, G.; Arndt, M.; Saba, M.; Mura, A.; Bongiovanni, G.; Sitter, H. Organic-organic heteroepitaxy of red-, green-, and blue-emitting nanofibers. *ACS Nano* **2010**, *4*, 6244−6250.
(30) Simbrunner, C.; Hernandez-Sosa, G.; Quochi, F.; Schwabegger, G.; Botta, C.; Oehzelt, M.; Salzmann, I.; Djuric, T.; Neuhold, A.; Resel, R.; Saba, M.; Mura, A.; Bongiovanni, G.; Vollmer, A.; Koch, N.; Sitter, H. Color tuning of nanofibers by periodic organic-organic heteroepitaxy. *ACS Nano* **2012**, *6*, 4629−4638.
(31) Djuric, T.; Hernandez-Sosa, G.; Schwabegger, G.; Koini, M.; Hesser, G.; Arndt, M.; Brinkmann, M.; Sitter, H.; Simbrunner, C.; Resel, R. Alternately deposited heterostructures of α-sexithiophene-para-hexaphenyl on muscovite mica(001) surfaces: crystallographic structure and morphology. *J. Mater. Chem.* **2012**, *22*, 15316−15325.
(32) Quochi, F.; Schwabegger, G.; Simbrunner, C.; Floris, F.; Saba, M.; Mura, A.; Sitter, H.; Bongiovanni, G. Extending the lasing wavelength coverage of organic semiconductor nanofibers by periodic organic-organic heteropitaxy. *Adv. Opt. Mater.* **2013**, *1*, 117−122.
(33) Resel, R. Crystallographic studies on hexaphenyl thin films - a review. *Thin Solid Films* **2003**, *433*, 1−11.
(34) Haber, T.; Muellegger, S.; Winkler, A.; Resel, R. Temperature-induced epitaxial growth modes of para-sexiphenyl on Au(111). *Phys. Rev. B* **2006**, *74*, 045419.
(35) Resel, R.; Salzmann, I.; Hlawacek, G.; Teichert, C.; Koppelhuber, B.; Winter, B.; Krenn, J.; Ivanco, J.; Ramsey, M. Structure and morphology of sexiphenyl thin films grown on aluminium (1 1 1). *Org. Electron.* **2004**, *5*, 45−51.
(36) Fleming, A. J.; Berkebile, S.; Ules, T.; Ramsey, M. G. Pre-nucleation dynamics of organic molecule self-assembly investigated by PEEM. *Phys. Chem. Chem. Phys.* **2011**, *13*, 4693−4708.
(37) Schroeder, P. G.; France, C. B.; Parkinson, B. A.; Schlaf, R. Orbital alignment at p-sexiphenyl and coronene/layered materials interfaces measured with photoemission spectroscopy. *J. Appl. Phys.* **2002**, *91*, 9095.
(38) Wang, Z.-H.; Kanai, K.; Iketaki, K.; Ouchi, Y.; Seki, K. Epitaxial growth of p-sexiphenyl film on highly oriented pyrolytic graphite surface studied by scanning tunneling microscopy. *Thin Solid Films* **2008**, *516*, 2711−2715.
(39) Chen, W.; Huang, H.; Thye, A.; Wee, S. Molecular orientation transition of organic thin films on graphite: the effect of intermolecular electrostatic and interfacial dispersion forces. *Chem. Commun.* **2008**, 4276−4278.
(40) Zhong, J. Q.; Huang, H.; Mao, H. Y.; Wang, R.; Zhong, S.; Chen, W. Molecular-scale investigation of C60/p-sexiphenyl organic heterojunction interfaces. *J. Chem. Phys.* **2011**, *134*, 154706.
(41) Baker, K.; Fratini, A.; Resch, T.; Knachel, H.; Adams, W.; Socci, E.; Farmer, B. Crystal structures, phase transitions and energy calculations of poly(p-phenylene) oligomers. *Polymer* **1993**, *34*, 1571.
(42) Athouel, L.; Froyer, G.; Riou, M. T.; Schott, M. Structural studies of parasexiphenyl thin films: importance of the deposition parameters. *Thin Solid Films* **1996**, *274*, 35−45.
(43) Horowitz, G.; Bachet, B.; Yassar, A.; Lang, P.; Demanze, F.; Fave, J.-L.; Garnier, F. Growth and characterization of sexithiophene single crystals. *Chem. Mater.* **1995**, *7*, 1337−1341.
(44) Vilar, M. R.; Horowitz, G.; Lang, P.; Pellegrino, O.; Botelho do Rego, A. M. Surface analysis of oligothiophene films using HREELS: molecular orientation effects. *Adv. Mater. Opt. Electron.* **1999**, *9*, 211−218.
(45) Magonov, S. N.; Reneker, D. H. Characterization of polymer surfaces with atomic force microscopy. *Annu. Rev. Mater. Sci.* **1997**, *27*, 175−222.
(46) Salzmann, I.; Duhm, S.; Opitz, R.; Johnson, R. L.; Rabe, J. P.; Koch, N. Structural and electronic properties of pentacene-fullerene heterojunctions. *J. Appl. Phys.* **2008**, *104*, 114518.
(47) de Oteyza, D. G.; Barrena, E.; Osso, J. O.; Sellner, S.; Dosch, H. Site-selective molecular organization in organic heterostructures. *Chem. Mater.* **2006**, *18*, 4212−4214.
(48) Zangwill, A. *Physics at Surfaces*; Cambridge University Press: Cambridge, U.K., 1988; p 21.
(49) Ishii, H.; Sugiyama, K.; Ito, E.; Seki, K. Energy level alignment and interfacial electronic structures at organic/metal and organic/organic interfaces. *Adv. Mater.* **1999**, *11*, 605−625.
(50) Duhm, S.; Heimel, G.; Salzmann, I.; Glowatzki, H.; Johnson, R.; Vollmer, A.; Rabe, J.; Koch, N. Orientation-dependent ionization energies and interface dipoles in ordered molecular assemblies. *Nat. Mater.* **2008**, *7*, 326.
(51) Oehzelt, M.; Grill, L.; Berkebile, S.; Koller, G.; Netzer, F.; Ramsey, M. The molecular orientation of para-sexiphenyl on Cu (110) and Cu(110) p(2 × 1)O. *ChemPhysChem* **2007**, *8*, 1707.
(52) Koller, G.; Winter, B.; Oehzelt, M.; Ivanco, J.; Netzer, F.; Ramsey, M. The electronic band alignment on nanoscopically patterned substrates. *Org. Electron.* **2007**, *8*, 63.
(53) Vogel, J.-O.; Salzmann, I.; Duhm, S.; Oehzelt, M.; Rabe, J. P.; Koch, N. Phase-separation and mixing in thin films of co-deposited rod-like conjugated molecules. *J. Mater. Chem.* **2010**, *20*, 4055−4066.
(54) Leclere, P.; Surin, M.; Viville, P.; Lazzaroni, R.; Kilbinger, A. F. M.; Henze, O.; Feast, W. J.; Cavallini, M.; Biscarini, F.; Schenning, A. P. H. J.; Meijer, E. W. About oligothiophene self-assembly: from aggregation in solution to solid-state nanostructures. *Chem. Mater.* **2004**, *16*, 4452−4466.
(55) Loi, M. A.; da Como, E.; Dinelli, F.; Murgia, M.; Zamboni, R.; Biscarini, F.; Muccini, M. Supramolecular organization in ultra-thin films of α-sexithiophene on silicon dioxide. *Nat. Mater.* **2005**, *4*, 81−85.
(56) Como, E. D.; Loi, M. A.; Murgia, M.; Zamboni, R.; Muccini, M. J-aggregation in α-sexithiophene submonolayer films on silicon dioxide. *J. Am. Chem. Soc.* **2006**, *128*, 4277.
(57) Sun, L.; Berkebile, S.; Weidlinger, G.; Denk, M.; Denk, R.; Hohage, M.; Koller, G.; Netzer, F. P.; Ramsey, M. G.; Zeppenfeld, P. Layer resolved evolution of the optical properties of α-sexithiophene thin films. *Phys. Chem. Chem. Phys.* **2012**, *14*, 13651−13655.
(58) Meinardi, F.; Cerminara, M.; Sassella, A.; Borghesi, A.; Spearman, P.; Bongiovanni, G.; Mura, A.; Tubino, R. Intrinsic excitonic luminescence in odd and even numbered oligothiophenes. *Phys. Rev. Lett.* **2002**, *89*, 157403.
(59) Salzmann, I.; Moser, A.; Oehzelt, M.; Breuer, T.; Feng, X.; Juang, Z.-Y.; Nabok, D.; Della Valle, R. G.; Duhm, S.; Heimel, G.; Brillante, A.; Venuti, E.; Bilotti, I.; Christodoulou, C.; Frisch, J.; Puschnig, P.; Draxl, C.; Witte, G.; Müllen, K.; Koch, N. Epitaxial growth of π-stacked perfluoropentacene on graphene-coated quartz. *ACS Nano* **2012**, *6*, 10874−10883.
(60) Sitter, H.; Andreev, A.; Matt, G.; Sariciftci, N. Hot wall epitaxial growth of highly ordered organic epilayers. *Synth. Met.* **2003**, *138*, 9−13.